Ultrasonics - Sonochemistry 48 (2018) 1–10

Contents lists available at ScienceDirect

Ultrasonics - Sonochemistry

journal homepage: www.elsevier.com/locate/ultson

Ultrasound-assisted synthesis of two novel [CuBr(diamine)$_2$·H$_2$O]Br complexes: Solvatochromism, crystal structure, physicochemical, Hirshfeld surface thermal, DNA/binding, antitumor and antibacterial activities

Ismail Warad[a,*], Firas F. Awwadi[b], Bahaa Abd Al-Ghani[a], Ashraf Sawafta[c], Naveen Shivalingegowda[d], Neartur Krishnappagowda Lokanath[e], Mohammad S. Mubarak[b], Taibi Ben Hadda[f], Abdelkader Zarrouk[f], Fuad Al-Rimawi[g], Abdallah Bani Odeh[h], Sameer A. Barghouthi[h]

[a] Department of Chemistry, Science College, An-Najah National University, P.O. Box 7, Nablus, Palestine
[b] Department of Chemistry, The University of Jordan, Amman 11942, Jordan
[c] Biology and Biotechnology Department, AN-Najah National University, P.O. Box 7, Nablus, Palestine
[d] Department of Physics, School of Engineering and Technology, Jain University, Bangalore 562 112, India
[e] Department of Studies in Physics, University of Mysore, Manasagangotri, Mysore 570 006, India
[f] Laboratoire Chimie Matériaux, FSO, Université Mohammed 1ER, Oujda 60000, Morocco
[g] Department of Chemistry, Faculty of Science and Technology, Al-Quds University, P.O. Box 20002, Al-Quds, Palestine
[h] Department of Medical Laboratory Sciences, Faculty of Health Professions, Al Quds University, Al Quds, Palestine

ARTICLE INFO

Keywords:
Cu(II) complexes
Diamine
Spectral
DNA
XRD
Hirshfeld surfaces
Antitumor activity

ABSTRACT

Two new hydrated monocationic Cu(II) complexes with 1,3-propylenediamine and 1,2-ethylenediamine of general formula [CuBr(N-N)$_2$·H$_2$O]Br were prepared. The complexes were identified by means of several spectroscopic tools (Uv-visible, IR and MS), thermally (TG/DTA) and CHN-elemental analysis. The three dimensional structure for complex **A** and **B** was provide by X-ray diffraction studies and showed the Cu(II) ion as 4 + 1 + 1 coordinated, four nitrogen atoms of the diamine ligands, one bromide ion and one H$_2$O semi-coordinated to the Cu(II) center, a typical *trans* effect is clearly observed in the two complexes. The molecular crystal structures are linked *via* several H-bonds like N_H…Br and N_H…O. Additionally, intra-molecular H-bonds of kind C_H…Br is observed; these interactions lead to crystal structure three dimensional architecture packing. Hirshfeld surfaces (HSA) analysis was served to figure out the inter-contacts and fingerprints atoms percentage. DNA-binding, antitumor and antibacterial effectiveness of the desired complexes were evaluated.

1. Introduction

Propylenediamine is an excellent primary diamine complexing reagent acts as an N,N-bidentate ligand, which is capable of coordinating with most of transition metal ions, including Cu(II) [1,2]. Diamine-Cu(II) complexes were found to serve as catalysts under mild conditions [3,4]. In addition, copper(II) complexes containing polydiamine ligands have shown high anti-cancer activity which may be due to their ability to inhibit DNA synthesis [5–13]. Recently, we have investigated the spectroscopic and the biological activity of [Cu(dipn)(N-N)]Br$_2$ with [dipn = dipropylene-triamine, propylene-diamine (pn) and N-N = ethylene-diamine (en)] [13].

Although copper complexes have important biological and chemotherapeutic activities, little is known about monocation Cu(II)-diamine complexes X-ray single crystal analysis [8–13]. In the scene of the wide attention in this type of Cu(II)/Cu(I) complexes, and due to their medical significance, we describe in this work the preparation, identification, X-ray analysis, and surface studies of new water soluble mono-cationic [CuBr(N-N)$_2$]$^+$Br$^-$ complexes where N-N = 1,3-propylene-diamine or 1,2-ethylene-diamine. In addition, the antibacterial, DNA and antitumor activities of the desired complexes versus various cancer-cell lines has been investigated.

2. Experimental

2.1. Chemicals

Reagents throughout this work were used as received from

* Corresponding author.
E-mail address: warad@najah.edu (I. Warad).

https://doi.org/10.1016/j.ultsonch.2018.05.009
Received 18 April 2018; Received in revised form 9 May 2018; Accepted 11 May 2018
Available online 12 May 2018
1350-4177/

Sigma–Aldrich Company.

2.2. Preparation of the desired complexes

Complexes **A** and **B** were prepared, in 80–90% yields. The diamine (2 mmoL) was dissolved in 10 mL distilled-water then inserted dropwise to the $CuBr_2{\cdot}2H_2O$ salt (1 mmoL in 10 mL ethanol) under ultrasonic vibration in interval of 10 min. The mixture was left for ~10 min until deep blue color solution is fixed and the reaction cools down. Under reduced pressure the solvent was evaporated and the blue powder product was washed well with iso-propanol and dichloromethane then deserted to dry.

2.2.1. Complex *A*

Yield 90%, m.p. = 185 °C. MS (*m/z*) $[M^+] = [CuBr(NN)_2]^+ = 292.2$ *m/z,* (291.8 theoretical). Elemental analysis Calc. for $[CuBr(NN)_2{\cdot}H_2O]Br$- which is equivalent to ($C_6H_{22}Br_2CuN_4O$): C, 18.50; N, 14.38 and H, 5.69. Found: C, 18.35; N, 14.22 and H, 5.71%. (IR, νcm^{-1}): 3380–3265 and 3160 ($\nu_{H\text{-}N}$), 2890 ($\nu_{C\text{-}H}$), 1565 ($\nu_{N\text{-}H}$), 1170 ($\nu_{N\text{-}C}$), 508 ($\nu_{Cu\text{-}N}$). UV–Vis./water: λ_{max} with (ε_{max}): 255 nm (1.20×10^3 1/ML) and 568 nm (2.90×10^2 1/ML).

2.2.2. Complex *B*

Yield 88%, m. p. = 165 °C. MS (*m/z*) $[M^+] = [CuBr(NN)_2]^+ = 262.2$ (263.65 theoretical). Elemental analysis Calc. for $[CuBr(NN)_2{\cdot}H_2O]Br$-which is equivalent to $C_4H_{18}Br_2CuN_4O$: C, 13.29; H, 5.02; N, 15.50 . Found: C, 13.24; H, 5.05; N, 15.31%, (IR, νcm^{-1}): 3375–3142 ($\nu_{H\text{-}N}$), 2925 ($\nu_{C\text{-}H}$), 1555 ($\nu_{N\text{-}H}$), 1175 ($\nu_{N\text{-}C}$), 515 ($\nu_{Cu\text{-}N}$). UV–Vis./water: λ_{max} (ε_{max}): 250 nm (1.27×10^3 1/ML) and 580 nm (3.11×10^2 1/ML).

2.3. Instruments

A TU-1901 DB UV–VIS spectrophotometer served to record the UV–visible analysis of complexes **A** and **B**, whereas IR was employed to record on a 1000 FT-IR Spectrophotometer PerkinElmer. EI-MS data were collected with the aid of a Finnigan 711A (8 kV) (PerkinElmer Inc., Waltham, MA, USA) instrument. Thermogravimetric analysis (TGA/DTA) was accomplished by using a TGA-7 PerkinElmer thermogravimetric analyzer. CHN-analysis was performed out with EuroVector EA3000. HSA analysis computed by CRYSTAL EXPLORER 3.1 software [14].

2.4. X-ray diffraction

Slow evaporation of complexes **A** and **B** ethanolic solution gave suitable crystals for XRD measurements. X-ray data of complex **A** were collected at a temperature of 293 K with the aid of a CCD diffractometer Bruker Proteum 2 equipped with an X-ray generator operating [15]. Crystal structure by means of the F^2 *SHELXS* and *SHELXL* programs [16]. Geometrical calculations performed using *PLATON* program [17], whereas the packing and molecular diagrams were carried out with the aid of the *MERCURY* software [18]. Diffraction Data set of complex **B** was collected on Xcalibur/Oxford Diffractometer using Mo tube as X-ray source (λ = 0.71073 Å). CrysAlis Pro software was served for absorption correction; the collected data was reduced to produce SHELX *hkl*-format files [19]. Both structures were refined and solved using SHELXTL program [20]. Data refinement and crystal structure details are illustrated in Table 1.

2.5. DNA binding

Experimental Abs. titration spectral was performed at pH 7.2 buffer solution of a Tris–HCl [5 mM Tris–HCl mixed with 50 mM NaCl] and with a Cu(II) complex concentration of 5.0×10^{-5} M. [CT-DNA] varied in between 0 and 1.0×10^{-4} M by keeping the volume constant (10.0 mL). Cu(II) complexes and CT-DNA mixture was allowed for 10 min to equilibrate at room temperature for all trial.

2.6. Biological assays

2.6.1. Preparation of stock solutions

A solution was made by resolving 20 mg of the complex in 20 mL of media (RPMI) supplemented with 1% penicillin streptomycin, 1% l-glutamine, 1% amphotericin B and 1% non-essential amino acid. This solution has a concentration of 0.5 mg/mL and was stored at 4 °C.

2.6.2. Cell lines

ATCC, HCT116 number: CCL-247, from human the epithelial tissue of the colon, PC3, ATCC number: CRL-1435, from human prostate and HepG2, ATCC number: HB-8065, from the human epithelial cells of the liver were grown in Dulbecco's modified Eagle's DMEM medium supplemented with 10% fetal calf serum, 1% penicillin streptomycin 1% l-glutamine, 1% non-essential amino acid and 1% amphotericin B. All cell lines were incubated at 37 °C in a humidified atmosphere of 5% CO_2 and 95% air.

2.6.3. Determination of cell viability

Cell viability was assayed by using the MTT method, the cells were seeded into 96-well plates at a density of 1×10^4 cells/well and allowed to incubate for 24 h. Cells were then incubated with increasing concentrations of test compounds for another 24 h. At the end of each treatment period, 10 μL of MTT (5 mg/mL in PBS) was added to each well and the microplate was incubated at 37 °C for 4 h. The medium with MTT was removed and 100 μL of DMSO was added to each well to dissolve the insoluble formazan crystals. Plates were incubated for 20 min at 37 °C and optical densities were measured at 570 nm with a reference wavelength of 630 nm as a background using a spectrophotometer plate reader.

2.6.4. MTT assay

Cells were seeded in 96-well plates at a concentration of 1×10^4 cells/well in 100 μL of complete media and incubated for 24 at 37 °C in a 5% CO_2 atmosphere to allow for cell adhesion. Stock solutions (1 mg/mL) of complexes **A** and **B** and then were diluted to achieve the following concentration: 1, 0.5, 0.250, 0.125, 0.065, and 0.03125 mg/mL. A 100 μL solution of each complex was added to a 100 μL solution of fresh medium in wells to give final concentrations of 1–0.03125 mg/mL. All assays were performed in triplicates. A control group containing no drug was run in each assay. Cytotoxicity was assessed using MTT solutions (5 mg/mL) and 100 μL of fresh, complete media which added to each well. Following four hour incubation, the medium was removed and the purple formazan precipitated in each well was sterilized in 100 μL DMSO. Absorbance was measured by means of a microplate reader at 570 nm and results are expressed as IC_{50} values directly calculated from % viability. Percentage (%) viability was calculated according to the following equation:

$$\%\ \text{viability} = (\text{OD in sample well/OD in control well}) \times 100\%(\text{OD} = \text{optical density}).$$

2.6.5. Antimicrobial assay

The antimicrobial activity of the two newly prepared complexes (A& B) were tested against the following microbial strains: Escherichia coli (ATCC 25922), Staphylococcus aureus (ATCC 25213), Klebsiella pneumoniae (ATCC 13883), Bacillus subtilis (ATCC 6633), and bacterial strains were stocked onto a nutrient agar slant. All slants were stored at 4 °C.

A disc diffusion method served to evaluate the antimicrobial activity of the prepared **A** and **B** complexes. Stock complexes **A** and **B** were initially dissolved in ethanol and sterilized by filtration using 0.45 lm

Table 1
Crystallographic data and structure refinement parameters for complexes.

	Complex **A**	Complex **B**
CCDC	1422015	1551373
Empirical formula	$C_6H_{20}N_4CuBr_2O$	$C_4H_{18}Br_2CuN_4O$
Formula weight	387.61	361.58
Temperature	293(2) K	293(2) K
Wavelength	1.54178 Å	0.71073 Å
Crystal system, space group	Monoclinic, $P2_1/c$	Monoclinic, *P 1 21/n 1*
Unit cell dimensions	a = 8.6858(5) Å	a = 6.4422(4) Å
	b = 15.0169(8) Å	b = 15.4116(9) Å
	c = 11.0250(6) Å	c = 12.0398(9) Å
	β = 112.668(2)°	β = 98.048(6)°
Volume	1326.95(13) $Å^3$	1183.59(13) $Å^3$
Z, Calculated density	4, 1.940 Mg/m^3	42.029 Mg/m^3
Absorption coefficient	9.230 mm^{-1}	8.567 mm^{-1}
$F_{(000)}$	764	708
Crystal size	0.26 × 0.27 × 0.28 mm	0.3 × 0.2 × 0.2 mm^3
Theta range for data collection	5.3–64.5°	3.15–26.30°
Limiting indices	$-7 \le h \le 10,\ -17 \le k \le 15,\ -12 \le l \le 9$	$-8 \le h \le 7,\ -19 \le k \le 17,\ -12 \le l \le 15$
Reflections collected/unique	5668/2107 [R(int) = 0.039]	5508/2385 [R(int) = 0.0394]
Final R indices [I > 2sigma(I)]	R1 = 0.0447, wR2 = 0.0634	R1 = 0.0422, wR2 = 0.0595
Data/restraints/parameters	2021/0/128	2385/1/115
Goodness-of-fit on F^2	1.11	0.989
Largest diff. peak and hole	1.22 and −0.90 e $Å^{-3}$	0.683 and −0.649 e $Å^{-3}$

membrane filters.

Sterile 6 mm diameter filter-paper discs was soaked with 0.2 mg/disc of the sterile complexes **A** and **B**, and were placed in triplicates onto Muller–Hinton agar (Oxoid, England) plates for bacterial strains. These plates were previously inoculated separately with 100 µL (1.0 10^8-CFU mL^{-1}) of fresh culture of bacteria suspension. The plates were incubated for 24 h at 37 °C. After incubation, the inhibition zone around each disc was measured and recorded. Recorded inhibition zones are an average of three replicates. Discs soaked with sterile water were used for negative control, while standard antibacterial tetracycline (30 µL/disc, Oxoid, Basingstoke, UK) was used as positive controls in the assay.

3. Results and discussion

3.1. Complexes *A* and *B* synthesis

As depicted in Scheme 1, pure Cu(II) complexes **A** and **B**, with [CuBr(N-N)$_2$·H_2O]Br as general formula, were prepared by reaction of 1,3-propylenediamine or 1,2-ethylenediamine with a copper(II) bromide salt in an ethanol–water mixture with 1:2 metal-to-ligand ratio under ultrasonic mode of vibration. As water-soluble bromide mono-cationic salts the desired complexes have been prepared in very good yields. Furthermore, these complexes were blue in color and the reactions that

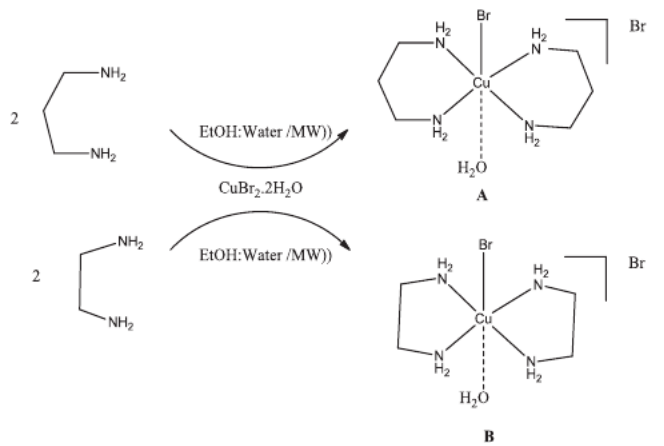

Scheme 1. Desired complexes synthesis.

led to their formation were highly exothermic. These newly synthesized complexes were identified with the aid of the CHN-elemental and various spectral analyses. The complexes structures were confirmed by XRD single analysis.

3.2. Determination of *A* and *B* complexes crystal structure

The asymmetric unit of the complexes **A** and **B** a mononuclear cationic molecular copper(II) complex $[Cu(N\text{-}N)_2)]^+$, the electrical charge is balanced by separate two bromide anion (Br^-) as depicted in Fig. 1. Also, the asymmetric includes mono-water molecule. Selected bond distances and angle values are illustrated in Table 2.

The central Cu(II) surrounds with four nitrogen atoms (N2, N6, N8, and N12) Cu(II) cations, then it completes its 4 + 1 + 1 coordination by forming semi-coordinated bonds with the water molecule and the separate bromide anion (Fig. 1). Since the water molecule coordinated the copper centre anti to the bromide ion with [H_2O…Cu…Br] angle ~170 (°) this making the best geometry around the metal in between square pyramid and octahedral structure.

The Cu…Br1 distance are quite long to be considered as coordinate bond, the Br–Cu bond length is 2.7089(7) Å and 2.948 Å for A and B (Table 2). The Cu–Br bond distance in coordinate bond is around 2.4 Å and is around 2.8 Å in Cu–Br semi-coordinated bond [21].

Similarly, The Cu…O distance is long in the both complexes, 3.53 Å and 2.71 Å in **A** and **B**, thus, the two complexes are better to be described as hydrates. However, trans effect is clearly obsereved in the two complexes, as the Cu…O distance is shorter in complex **A**, and Cu-Br is shorter in complex **B** (Table 2).

Hydrogen bonding interactions (N_H…O, O_H…Br, and N_H…Br) connect the cationic and anionic units to form layer structures in both complexes (Fig. 2); the layer structure lie parallel the bc crystallographic plane in complex **A** and ac in complex **B**. Summarized data of these interactions are recorded in Table 3. Then, subsequently these layers are linked *via* weaker non classical C_H…O and C_H…Br H-bonding interactions to form the final three dimensional structures.

3.3. 3D-Hirshfeld surfaces analysis comparison between complexes *A* and *B*

Displayed in Fig. 3 are the Hirshfeld surfaces of complex **A** and **B**. Hydrogen bonds and other sufficient intercontacts were indicated by red spots over whole molecules surface [22–26]. Several dark-red spots on the d_{norm} of both complexes reflect the short interatomic contacts,

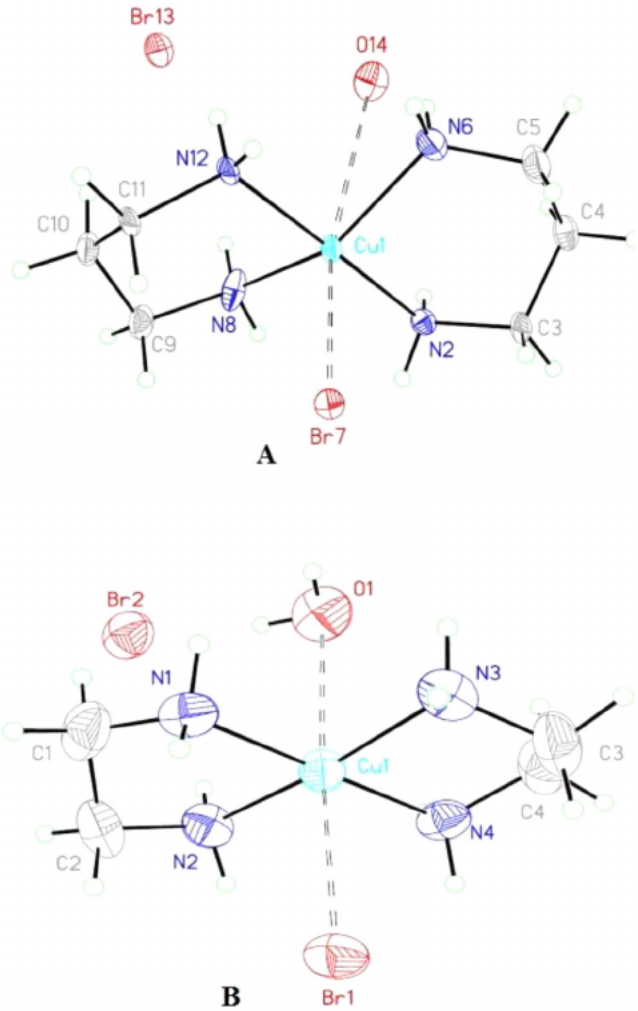

Fig. 1. ORTEP of complexes **A** and **B**.

Table 2
Chosen angles (°) and bond distance (Å) for complexes **A** and **B**.

Complex **A**		Complex **B**	
Cu(1)–N(2)	2.011(4)	Cu(1)–N(1)	2.002(3)
Cu(1)–N(6)	2.053(4)	Cu(1)–N(2)	2.023(3)
Cu(1)–N(8)	2.051(4)	Cu(1)–N(3)	2.017(3)
Cu(1)–N(12)	2.020(4)	Cu(1)–N(4)	1.996(3)
Cu(1)–Br(7)	2.7089(7)	Cu(1)–Br1	2.948
Cu(1)–O(14)	3.530	Cu(1)–O1	2.719
N(2)–Cu(1)–N(12)	179.01(13)	N(4)–Cu(1)–N(1)	179.43(15)
N(2)–Cu(1)–N(8)	89.50(15)	N(1)–Cu(1)–N(3)	94.92(15)
N(12)–Cu(1)–N(8)	90.18(15)	N(4)–Cu(1)–N(3)	84.51(15)
N(2)–Cu(1)–N(6)	90.30(15)	N(1)–Cu(1)–N(2)	84.69(15)
N(12)–Cu(1)–N(6)	90.52(15)	N(4)–Cu(1)–N(2)	95.87(15)
N(8)–Cu(1)–N(6)	143.54(17)	N(3)–Cu(1)–N(2)	173.64(15)
N(2)–Cu(1)–Br(7)	87.27(9)	N(1)–Cu(1)–Br(1)	87.31
N(12)–Cu(1)–Br(7)	91.89(10)	N(2)–Cu(1)–Br(1)	97.20
N(8)–Cu(1)–Br(7)	101.87(11)	N(3)–Cu(1)–Br(1)	89.87
N(6)–Cu(1)–Br(7)	114.54(13)	N(4)–Cu(1)–Br(1)	92.73
Br(7)–Cu(1)–O(14)	170.23	Br(1)–Cu(1)–O(1)	173.32

whereas long interactions rise as light-red spots. At the same level of calculation complex **B** revealed more short contacts, 7 red spots were collected on the Hirshfeld surface of **B**, while 5 spots only collected in complex **A** surface. In both complexes the spots are close to the polar H-N, H-O and Br-Cu functional groups creating source of ports to the neighbour molecules.

Two strong types of H-bond (N_H…Br and N_H…O) interactions

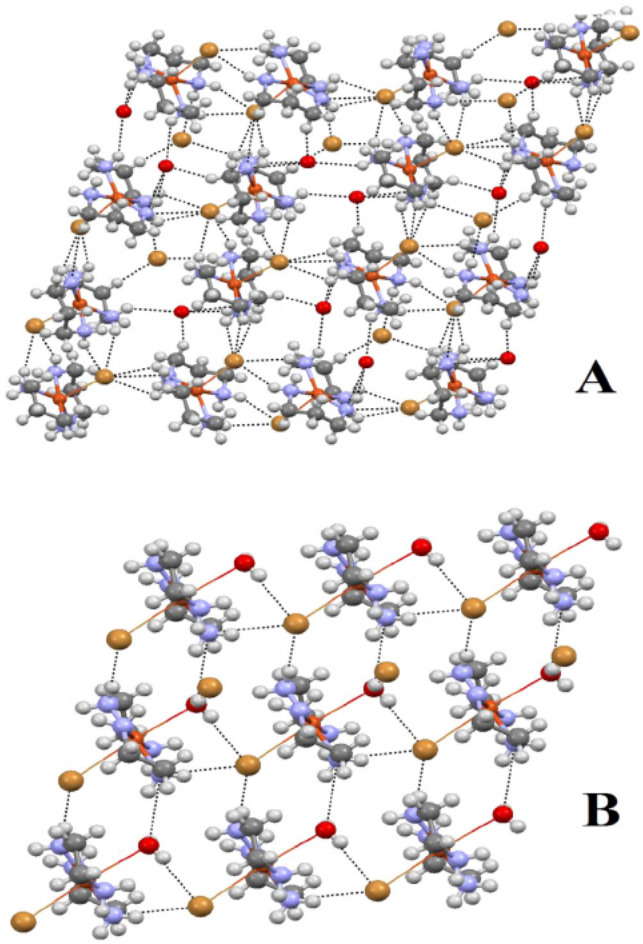

Fig. 2. Layer structures of complex **A** and **B**. Hydrogen bonding interactions are shown by dotted lines.

Table 3
Hydrogen bonding interactions angles (°) and distances (Å).

Complex **A**		Complex **B**	
H6A…O14	2.165	H2…Br1	2.536
N6-…O14	2.990	O1…Br1	3.289
N6–H16A…O14	151.9	O1–H2…Br1	165.1
H6B…Br7	2.750	H1…Br2	2.319
N6…Br7	3.399	O1…Br2	3.250
N6–H6B…Br7	130.0	O1–H1…Br2	172.4
		H1D…Br1	2.542
		N1…Br1	3.417
		N1–H1D…Br1	164.1
		H1A…O1	2.363
		N1…O1	3.170
		N1–H1A…O1	149.0
		H4D…Br1	2.563
		N1…Br1	3.459
		N1–H4D…Br1	173.5

were computed as deep-red spots on complex **A** surface. On the complex **B** surface, the same interactions together with new N_H…….Br H-bond were recorded. This result is in agreement with the hydrogen bonding interactions collected by X-ray structure analysis.

The 2D-Finger-print lots on the HSA surfaces in both complexes showed the H-inter-contacts percentage in the subsequent: H……. H > H...Br > H...O, where no H…C, H…N and H…Cu interactions were detected (Fig. 4).

In complex **A** the H…H major contribution was found to be higher that complex **B**, H…Br was also higher in complex **A**, while H…O

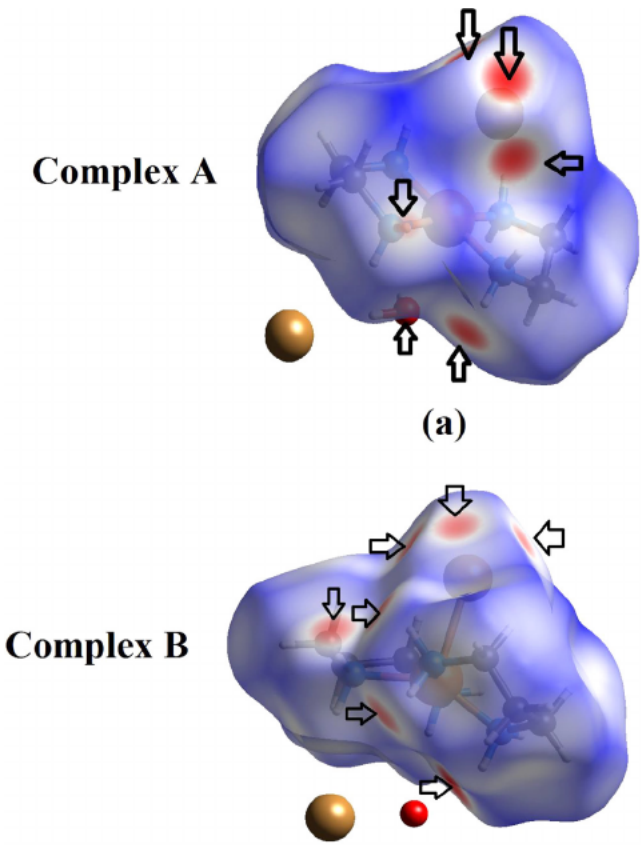

Fig. 3. d_{norm} Hirshfeld surface of both complexes.

contribution is more in complex **B** than **A** and H…X (X = N, C and Cu) contributions in both complexes were found to be zero, as seen in Fig. 5.

3.4. Mass spectrum, elemental analyses, conductivity and water solubility

The mass spectra, elemental analysis, conductivity and water solubility of the desired complexes are consistent with their mono-cationic $[CuBr(NN)_2{\cdot}H_2O]Br$ proposed formula (see experimental part), which was already confirmed by X-ray single crystals measurements for both complexes. For example, complex **A** elemental analysis Calc. for $C_6H_{22}Br_2CuN_4O$: C, 18.50N; 14.38 and H, 5.69. Found: C, 18.35; H, 5.71; N, 14.22%. This result is consistent with the existence of one water molecule in lattice of the desired complexes reflecting the expected general formula $[CuBr(NN)_2{\cdot}H_2O]Br$. TOF-MS of complex **A** is in agreement with $[CuBr(NN)_2]^+$ formula showing $[M^+] = 292.2\ m/z$, (291.8 theoretical) as in Fig. 6.

The water solubility of complex **A** was found to be 0.045 mg/L at RT and the conductivity of aqueous (1×10^{-3} M) at RT equal to $205\ \Omega^{-1}\ cm^2\ mol^{-1}$, complex **B** showed slightly higher water solubility 0.065 mg/L at RT and the conductivity of aqueous 1×10^{-3} M found to be $225\ \Omega^{-1}\ cm^2\ mol^{-1}$ at RT.

3.5. Ft-Ir

FT-IR of complexes **A** and **B** are given in Fig. 7. IR revealed absorption bands in 3300–3200 and 1650–1520 cm^{-1} assigned to ν_s/ν_{as} (N–H) and ν_b(N–H), respectively; such sets are slightly transmitted to less wavenumbers, and are sharper than those of the free primary diamine, indicating the coordination of the $-NH_2$ groups with Cu(II) center [27]. The strong bands 2950–2845 cm^{-1} are related to the C–H stretching vibrations of CH_2 sp^3 groups in the diamine ligand [28]. In addition, the peak at 610–500 cm^{-1} is sited to $\nu_{(Cu\text{-}N)}$ vibration [29].

3.6. UV Vis. Spectral analysis

Complexes **A** and **B** UV–Vis. spectra were performed in distilled water at RT. The complexes exhibited absorption bands at λ_{max} = 250 nm (complex **A**) and 245 nm (complex **B**), as seen in Fig. 8, corresponding to to * transition. Additionally, the absorption bands at $_{max}$ = 568 nm (complex **A**) and 577 nm (complex **B**) and in the blue color region are due to the d-d electronic transition [30–33].

3.7. Solvatochromism of complex A

The low solubility of the complexes limited the solvents to polar solvents which can be used to evaluate solvatochromism phenomena in these compounds, for this reason, only water; EtOH, DMF, and DMSO were investigated. Absorption spectra of **A** in the chosen solvents are seen in Fig. 9. The visible spectra of this complex in different solvents reveal absorption bands in the region 450–800 nm. Solvatochromic probes in selected solvents are ascribed to strong expected Jahn–Teller distortion of (d^9) copper(II) ion [30–34].

Bathochromic color changes shift was observed and is attributed to water-polar solvent displacement causing semi-octahedral coordination with the Cu(II) center, which is in consistent with the solvatochromism mechanism of such complexes [30]. Accordingly, the visible bands chemical shift increases linearly with increase in Gutmann's (DN) donor-number of solvents. In Fig. 10 the linear mode of λ_{max} (complex **A**) *vis.* DN with $R^2 = 0.9846$ reflected the degree of the electronic poverty as well as Lewis acidity natural of such complexes [32].

3.8. Thermogravimetric analyses of complex A

In the current investigation, we have performed TG/DTG analyses to collect input upon the thermal-stability of complex **A**. To perform these measurements, the temperature was increased from 0 to 900 °C at 10 °C/min. heating rate. Displayed in Fig. 11 are the resulting TGA curves for complex **A**.

Results from thermogravimetric analysis of the complex revealed the occurrence of three consecutive mass losses; dehydration, organic ligand pyrolysis, inorganic ligand de-structure to metal oxide residue formation [13]. The first step which involved loss of uncoordinated water molecule was at ~100 °C. In the second decomposition stage, the diamine ligand was lost in the temperature range of 200–280 °C to form $CuBr_2$. At higher temperatures, the complex undergoes further decomposition steps that lead finally to produce copper(II)-oxide (CuO); this stage happen in 580–620 °C temperature range. The formation of CuO was confirmed by FT-IR solid state measurement; the broad band of $\nu_{Cu=O}$ at ~ 500 cm^{-1} was detected [35].

3.9. CT-DNA binding affinity of complexes

3.9.1. Absorption titration

UV visible absorption titration spectroscopy is one versatile method to estimate DNA-binding affinity [36]. The complexes affinity toward CT-DNA binding was followed by UV-titrations in Tris–HCl buffer solution. Typically, changes are expected in UV spectra of the desired compound by drug-DNA binding [37–42]. Fig. 12 showing the UV–-Visible spectra titration of complex **A** upon CT-DNA addition.

$5x10^{-5}$ M of Cu(II)-complexes were treated with several DNA concentrations from 0 to 1×10^{-4} M in order to monitor the decrease in absorption at λ_{max} = 250 nm, as seen in Fig. 12. To estimate the binding ability of investigated complexes by calculation of K_b for both complexes. K_b values were evaluated by observing the variations in Abs. *vs.* CT-DNA concentrations by employing the following equation:

$$[DNA]/(_a - _f) = [DNA]/(_b - _f) + 1/K_b\,[DNA]/(_b - _f)$$

[DNA] is the DNA concentrations, ε_f, ε_b and ε_a, are the free-, metal-bound-complex and apparent extinction coefficients, respectively. K_b is

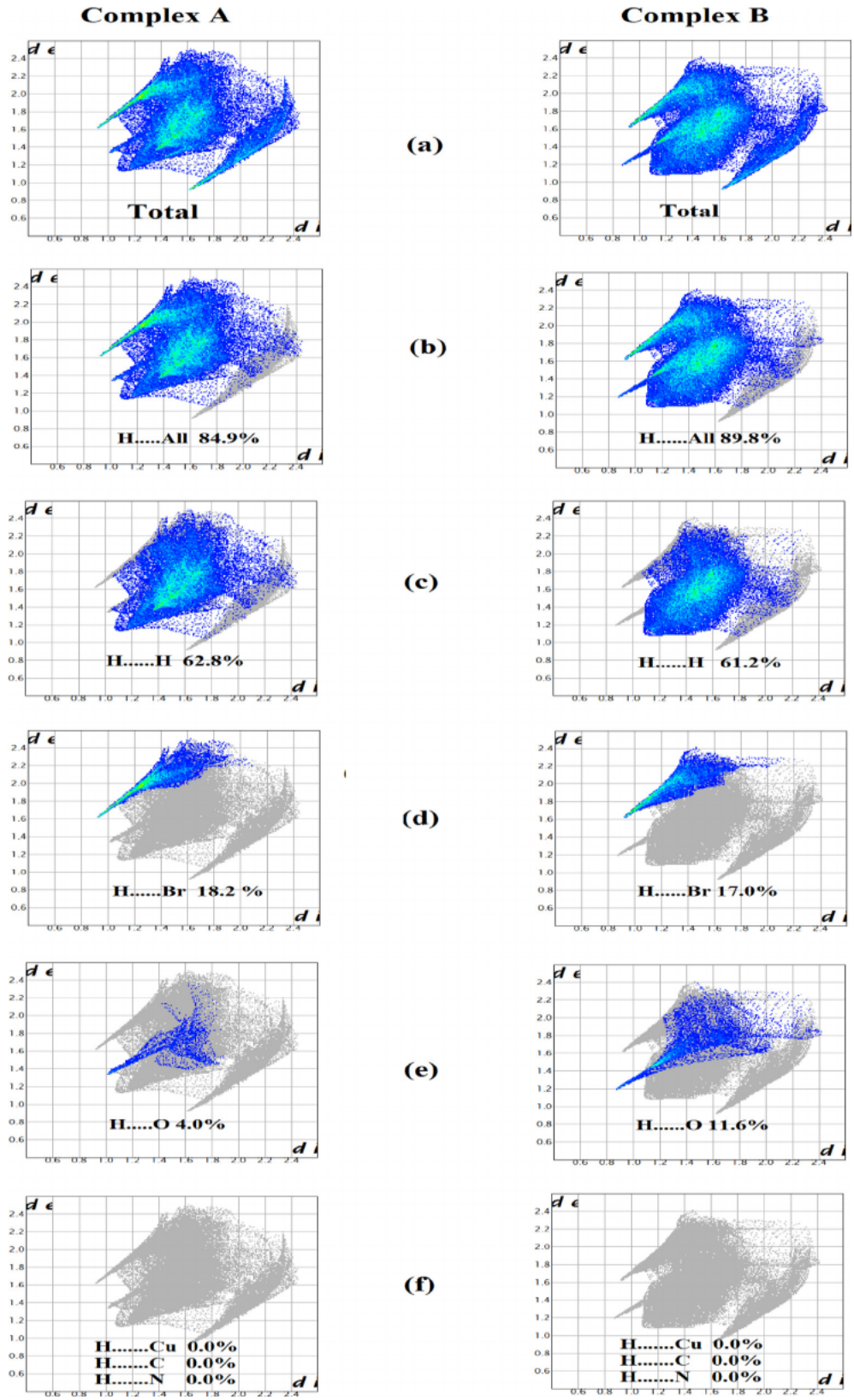

Fig. 4. Fingerprint of both complexes.

the intrinsic binding constant. K_b was calculated from the slope to intercept when $[DNA]/(\varepsilon_a-\varepsilon_f)$ *vs* [DNA] was plotted. K_b for **A** = $1.30 \times 10^4\,M^{-1}$ (Fig. 12) and $1.5 \times 10^4\,M^{-1}$ for **B**. These results are comparable to those collected by other researchers for similar Cu(II) complexes [35–38].

3.9.2. Viscosity test

To estimate the Cu-DNA binding ability, viscosities of DNA solution

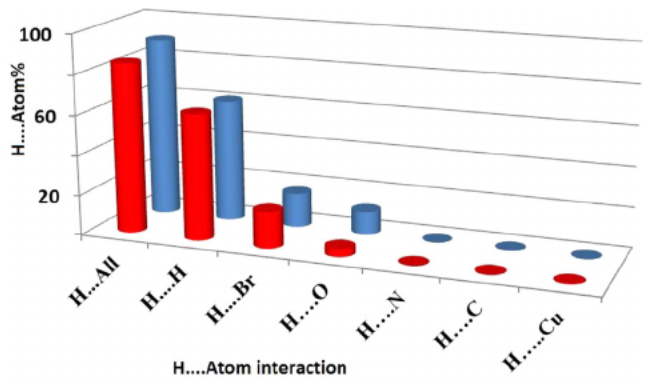

Fig. 5. H.....Atoms contributions percentages of a complex **A** and b complex **B**.

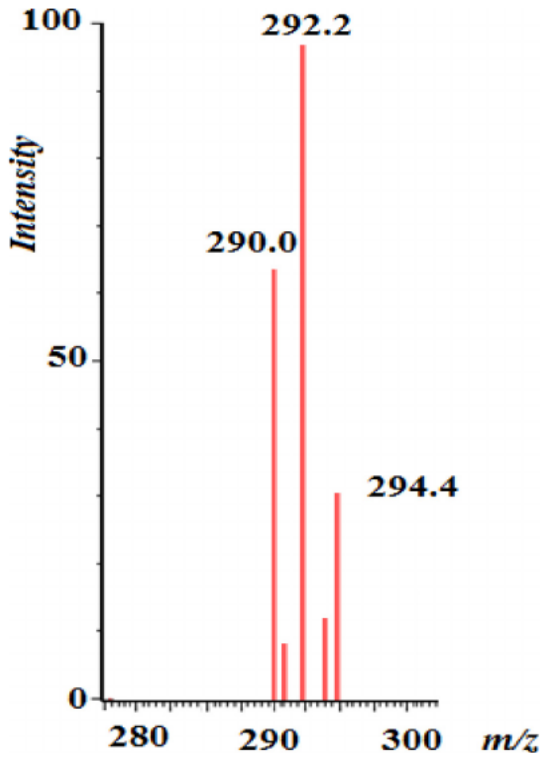

Fig. 6. TOF-MS of complex **A**.

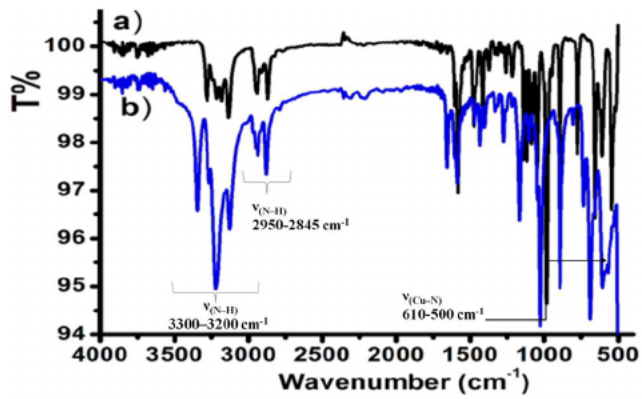

Fig. 7. The FT-IR of (a) complex **A** and (b) complex **B**.

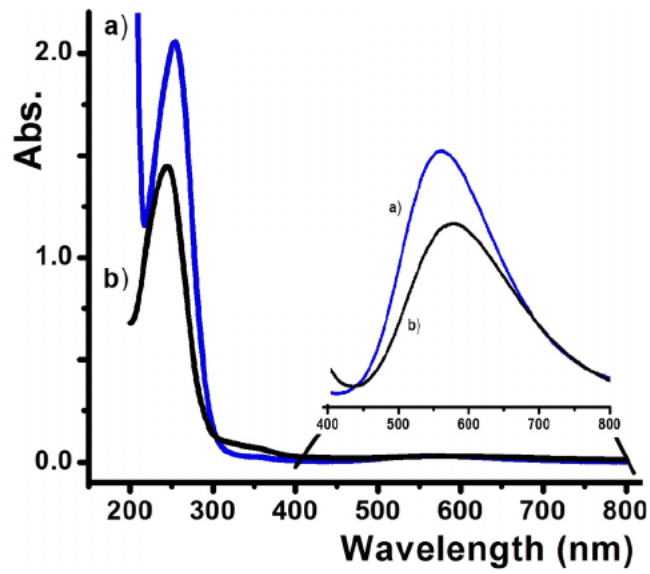

Fig. 8. UV–Vis spectra of 1×10^{-4} M: a) complex **A**, and b) complex **B** in H_2O and at room temperature.

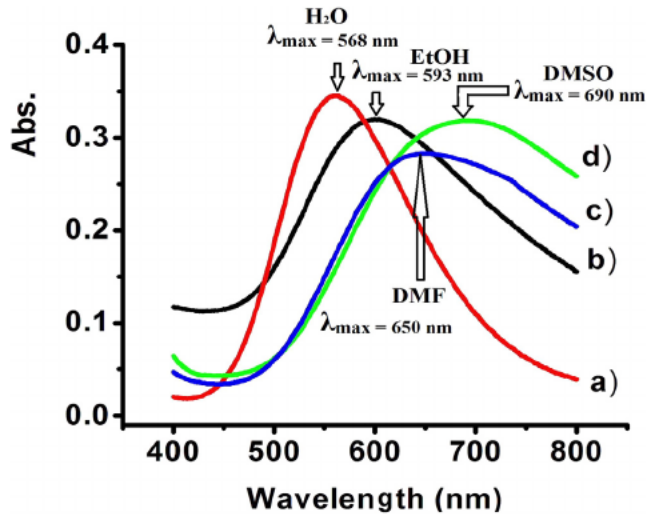

Fig. 9. Abs. spectra of **A** in selected solvents.

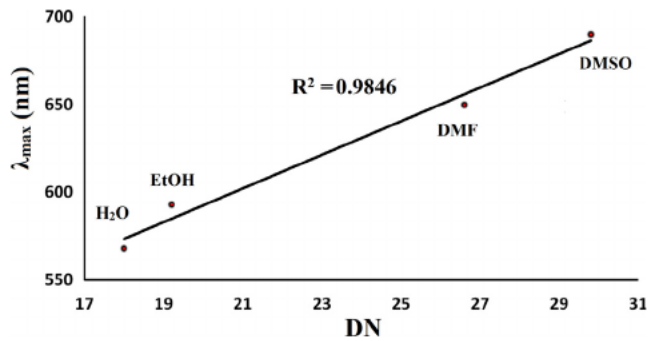

Fig. 10. Dependence of λ_{max} of complex **A** on the solvent's Gutmann donor number values.

before and after complexes were evaluated. The intercalative binding mode proposes that the DNA-helix will be elongated owing to Cu(II)-binding leading to arise in the M. Wt. which expected to enhance the viscosity [38]. The complexes insertion effect on the DNA viscosity was illustrated in Fig. 13.

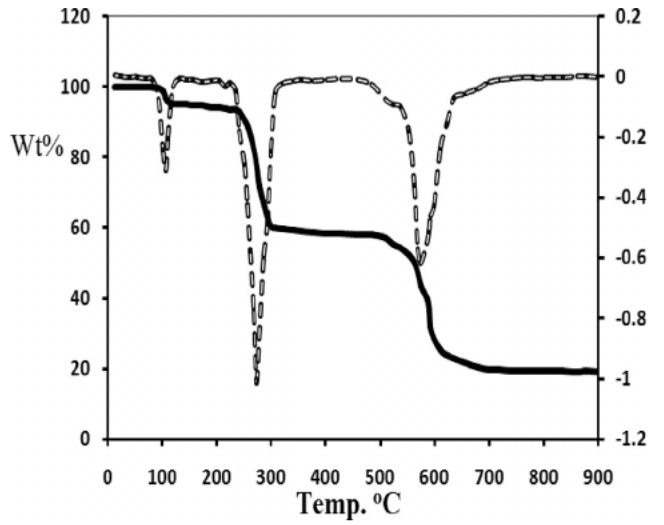

Fig. 11. TG-DTG thermal curve of complex **A** (TG is the thick solid line, other line represents DTG).

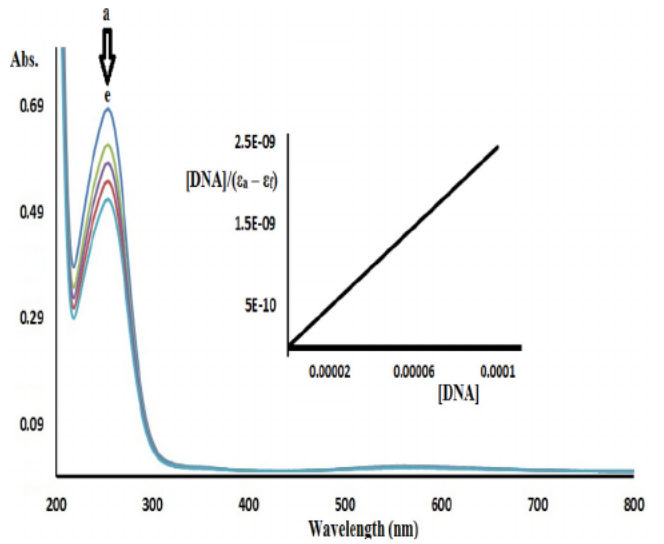

Fig. 12. (a) 5.0×10^{-5}M of **A** UV–Vis. spectra interacted with 0, 1.0×10^{-6}, 5.0×10^{-6}, 1.0×10^{5} and 1.0×10^{-4}M (a e) [DNA] at RT. (b) Draw of [DNA] against $[DNA]/(\varepsilon_a - \varepsilon_f)$ at $\lambda_{max} = 250$ nm to calculate the K_b intrinsic binding-constant.

Increasing Cu(II) concentrations of both complexes revealed enhancement in the DNA relative viscosity with non-linear ratio (Fig. 13). Such increasing reflected relatively a high degree of DNA binding the Cu(II) complexes. Results propose **B** bind the DNA better than **A**, in addition, such complexes bind the DNA through the intercalation mode [36–40].

3.10. Proliferation assay

The MTT cell assay is reasonable technique to evaluate the cell proliferation-rate [13].

Data collected from the this study by the MTT assay indicated that both complexes are with high inhibitory effects on the accession of HCT116 colon, HepG2 liver, and PC-3 prostate cancer cells [36–38]. In addition, the cytotoxicity of these complexes reduces in a time dependent fashion. Furthermore, the IC_{50} values for complexes were found to be 31.25 μg/mL (complex **B**) and (complex **A**) 30.55 μg/mL at 24 h of treatment. However, more studies are required to establish the efficacy and safety of these compounds and to have a structure-activity profile

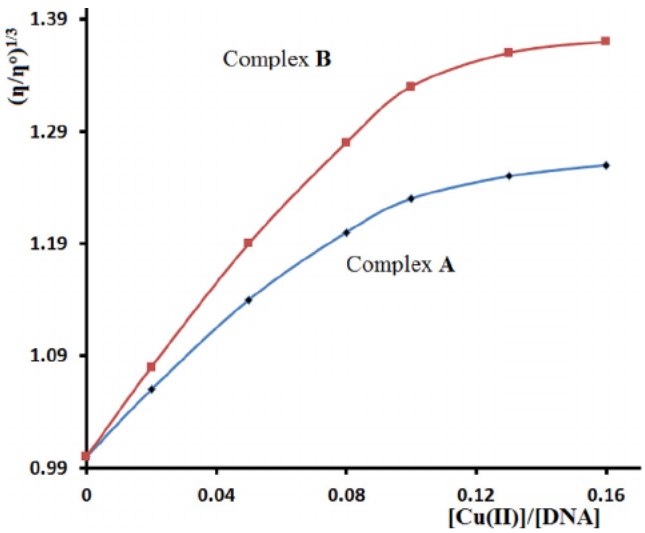

Fig. 13. Effect of rising copper(II) complexes concentrations on the relative DNA viscosity at RT, [DNA] = 4.0×10^{-4} M.

for these complexes. Similarly, it is equally important to have an idea about their biological stability. Furthermore, we performed survival studies where cells were incubated, separately with complexes **A** and **B**, and then washed to get rid of Cu(II) complexes. The cell survival was determined at complex concentrations ranging from 1 to 0.03215 mg/mL). At these concentrations, complex **A** was able to kill 78, 82, 84, 83, 86, and 87% of the HCT116 cells, respectively, as depicted in Fig. 14.

Moreover, complex **B** at the same concentrations was able to kill 78, 81, 82, 82, 83, and 84% of the HCT116 cells, respectively, as shown in Fig. 14.

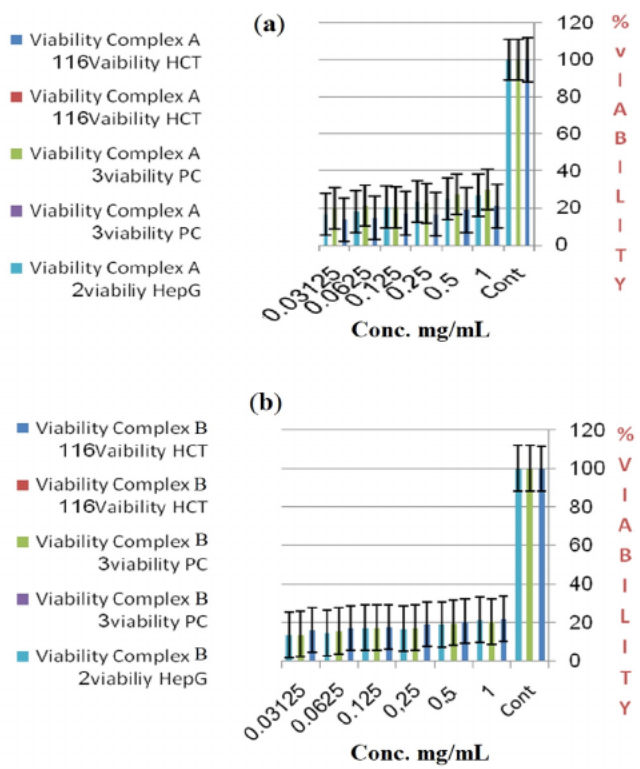

Fig. 14. (a) Inhibitory effects of complex **A** and (b) complex **B** on the proliferation of HepG2 liver cancer cells, PC3 and HCT 116.

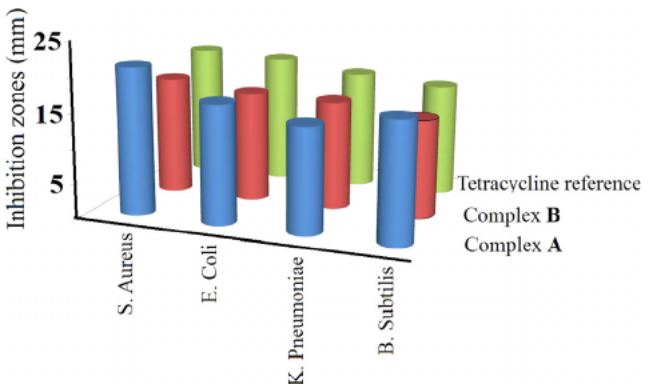

Fig. 15. Antimicrobial inhibition zones (mm) of 1 mg/ml of complexes **A** and **B** against several microbial strains.

3.11. Antimicrobial studies

The antimicrobial activity and inhibition efficiencies of the two new designed complexes **A** and **B** were tested against two Gram-positive (S. aureus and B. subtilis) and two Gram-negative bacteria (K. pneumonia and E. coli) (Fig. 15).

The highest activity of the complex **A** was against S. aureus with an inhibition zone of 21.3 mm; complex **A** also exhibited a strong activity against K. pneumonia, E. coli and B. subtilis, showing inhibition zones of 17.1, 15.2 and 17.2 mm, respectively. Complex **A** exhibited a strong promising activity against S. aureus and B. subtilis, even better than the Tetracycline antibiotic, as seen in Fig. 15.

The highest activity of complex **B** was against S. aureus with an inhibition zone of 17.2 mm; complex **B** exhibited strong activity against E. coli, K. pneumonia and B. subtilis, with inhibition zones of 15.9, 15.6 and 14.1 mm, respectively.

In general, complex **A** revealed a higher antibacterial activity compared to complex **B**., may be due to structure shape activities since complex **A** is with two six hetero-membered rings while complex **B** is with two five hetero-membered rings. Nevertheless, both complexes showed very good results as antibacterial agents.

4. Conclusions

We synthesized mono-cationic $[CuBr(N\text{-}N)_2{\cdot}H_2O]Br$ complexes using 1.2- and 1,3-diamines ligands under ultrasonic mode of vibration. The structures of the **A** and **B** complexes were solved by XRD crystallography then identified by FT-IR, MS, UV–visible, elemental and thermal test. In X-ray solved structures complexes one water molecule formed semi-coordinated bond to Cu centre $[H_2O\ldots Cu\ldots Br]$ making the geometry in between square pyramid and octahedral structure. Hirshfeld surfaces analysis of both complexes reflected an excellent agreement with XRD intercontacts data.

Complex **A** established positive solvatochromism using several polar solvents with different DN number due to water-polar solvents coordination replacement at the axial site of the Cu(II) centre. The CT-DNA binding interaction mode with the **A** and **B** compounds was evaluated by UV–VIS. and viscosity analysis, the results revealed a high CD-DNA binding consisting with the antitumor behaviour of the molecules against several types of cancer cells. Promising anti-microbial activities of both **A** and **B** complexes against several Gram-positive/negative bacteria were observed.

A. Supplementary material

Crystallographic data for complex **A** and **B** have been deposited with the Cambridge Crystallographic Data Centre as supplementary publication number CCDC 1422015 and 1551373, respectively. Copies of this information may be obtained free of charge via www.ccdc.cam.ac.uk/conts/retrieving.html (or from the CCDC, 12 Union Road, Cambridge CB2 1EZ, UK; Fax: +44-1223-336033; e-mail deposit@ccdc.cam.ac.uk).

References

[1] T.J.P. McGivern, S. Afsharpour, C.J. Marmion, Copper complexes as artificial DNA metallonucleases: from Sigman's reagent to next generation anti-cancer agent, Inorg. Chimica Acta 472 (2018) 12–39.
[2] T. Rosu, E. Pahontu, C. Maxim, R. Georgescu, N. Stanica, A. Gulea, Some new Cu (II) complexes containing an ON donor Schiff base: synthesis, characterization and antibacterial activity, Polyhedron 30 (2011) 154–162.
[3] R. Kowalczyk, L. Sidorowicz, J. Skarzewski, Asymmetric Henry reaction catalyzed by chiral secondary diamine-copper (II) complexes, Tetrahedron Asymmetry 19 (2008) 2310–2315.
[4] B. Tan, P.J. Chua, Y. Li, G. Zhong, Organocatalytic asymmetric tandem michael – henry reactions: a highly stereoselective synthesis of multi-functionalized cyclohexanes with two quaternary stereo-centers, Org. Lett. 10 (2008) 2437–2440.
[5] S. Koohzad, H. Golchoubian, Z. Jaglicic, Structural, solvatochromism and magnetic properties of two halogen bridged dinuclear copper(II) complexes: a density functional study, Inorg. Chim. Acta 473 (2018) 60–69.
[6] M.K. Hema, C.S. Karthik, I. Warad, N.K. Lokanath, Abdelkader Zarrouk, K. Kumara, K.J. Pampa, P. Mallu, Regular square planer bis-(4,4,4-trifluoro-1-(thiophen-2-yl) butane-1,3-dione)/copper(II) complex: *Trans/cis*-DFT isomerization, crystal structure, thermal, solvatochromism, hirshfeld surface and DNA binding analysis, J. Mol. Struct. 1157 (2018) 69–77.
[7] S. Tabassum, S. Amir, F. Arjmand, S. Pettinari, F. Marchetti, N. Masciocchi, G. Lupidi, R. Pettinari, Mixed-ligand Cu(II)–vanillin Schiff base complexes; effect of coligands on their DNA binding, DNA cleavage, SOD mimetic and anticancer activity, Eur. J. Med. Chem. 60 (2013) 216–232.
[8] X.B. Fu, Z.H. Lin, H.F. Liu, X.Y. Le, A new ternary copper (II) complex derived from 2-(2′-pyridyl) benzimidazole and glycylglycine: synthesis, characterization, DNA binding and cleavage, antioxidation and HSA interaction, Spectrochim. Acta A 122 (2014) 22–33.
[9] M. Gonzalez-Alvarez, A. Pascual-Alvarez, L.D. Agudo, A. Castineiras, M. Liu-Gonzalez, J. Borras, G. Alzuet-Pina, Mixed-ligand copper (II)–sulfonamide complexes: effect of the sulfonamide derivative on DNA binding, DNA cleavage, genotoxicity and anticancer activity, Dalton Trans. 42 (2013) 10244–10259.
[10] V.M. Manikandamathavan, V. Rajapandian, A.J. Freddy, T. Weyhermuller, V. Subramanian, B.U. Nair, Effect of coordinated ligands on antiproliferative activity and DNA cleavage property of three mononuclear Cu(II)-terpyridine complexes, Eur. J. Med. Chem. 57 (2012) 449–458.
[11] W.J. Song, Q.Y. Lin, W.J. Jiang, F.Y. Du, Q.Y. Qi, Q. Wei, Synthesis, interaction with DNA and antiproliferative activities of two novel Cu(II) complexes with norcantharidin and benzimidazole derivatives, Spectrochim. Acta A 137 (2014) 122–128.
[12] M. Al-Noaimi, A. Nafad, I. Warad, R. Alshwafy, A. Husein, W.H. Talib, T. Ben Hadda, Heterotrimetallic Ru(II)/Pd(II)/Ru (II) complexes: Synthesis, crystal-structure, spectral characterization, DFT calculation and antimicrobial study, Spectrochim. Acta Part A 122 (2014) 273–282.
[13] M. Al-Noaimi, M.I. Choudhar, F.F. Awwadi, W.H. Talib, T. Ben Hadda, S. Yousuf, A. Sawafta, I. Warad, Characterization and biological activities of two copper (II) complexes with dipropylenetriamine and diamine as ligands, Spectrochim. Acta Part A Mol. Biomol. Spectrosc. 127 (2014) 225–230.
[14] S.K .Wolff, D.J. Grimwood, J.J. McKinnon, D. Jayatilaka, M.A. Spackman, Crystal Explorer 2.1 University of Western Australia, Perth, Australia, 2007.
[15] A.P.E.X. Bruker, SAINT PLUS, Bruker AXS Inc., Madison, Wisconsin, USA, 2012.
[16] G.M. Sheldrick, A short history of SHELX, Acta. Cryst. A64 (2008) 112–122.
[17] A.L. Spek, PLATON, an integrated tool for the analysis of the results of a single crystal structure determination, Acta. Cryst., A 46 (1990) C34.
[18] C.F. Macrae, I.J. Bruno, J.A. Chisholm, P.R. Edgington, P. McCabe, E. Pidcock, L. Rodriguez-Monge, R. Taylor, J. van de Streek, P.A. Wood, Mercury CSD 2.0-new features for the visualization and investigation of crystal structures, J. Appl. Cryst. 41 (2008) 466–470.
[19] CrysAlisPro, Agilent Technologies, Yarnton, Oxfordshire, UK, 2011.
[20] A.P.E.X. Bruker, SAINT PLUS, Bruker AXS Inc., Madison, Wisconsin, USA, 2002.
[21] F.F. Awwadi, R.D. Willett, S.F. Haddad, B. Twamley, The electrostatic nature of aryl – bromine – halide synthons: the role of aryl-bromine-halide synthons in the crystal structures of the *trans-bis*-(2-bromopyridine)dihalocopper(II) and trans-bis (3-bromopyridine) dihalocopper (II) complexes, Cryst. Growth Des. 6 (2006) 1833–1838.
[22] M.A. Spackman, D. Jayatilaka, Hirshfeld surface analysis, Cryst. Eng. Comm. 11 (2009) 19–32.
[23] M.A. Spackman, J.J. McKinnon, Fingerprinting intermolecular interactions in molecular crystals, Cryst. Eng. Comm. 4 (2002) 378–392.
[24] I. Warad, A. Barakat, Synthesis, physicochemical analysis of two new hemilabile ether-phosphine ligands and their first stable bis-ether-phosphine/cobalt(II) tetrahedral complexes, J. Mol. Struct. 1134 (2017) 17–24.
[25] A. Barakat, S.M. Soliman, H.A. Ghabbour, M. Ali, A.M. Al-Majid, A. Zarrouk, I. Warad, Intermolecular interactions in crystal structure, Hirshfeld surface, characterization, DFT and thermal analysis of 5-((5-bromo-1H-indol-3-yl)methylene)-1,3-dimethylpyrimidine-2,4,6-(1H,3H,5H)-trione Indole, J. Mol. Struct. 1137 (2017) 354–361.

[26] I. Warad, F. Al-Rimawi, A. Barakat, S. Affouneh, N. Shivalingegowda, N.K. Lokanath, I.M. Abu-Reidah, Synthesis, spectral, thermal, crystal structure, Hirschfeld analysis of [bis(triamine)Cadimium(II)][Cadimum(IV)tetra-bromide] complexes and their thermolysis to CdO nanoparticles, Chem. Central J. 10 (2016) 1–11.
[27] S. Nawaz, A. Ghaffar, W. Zierkiewicz, M. Khurram, M. Tahir, A.A. Isab, S. Ahmad, DFT studies of copper(II) complexes of cis-1,2-diaminocyclohexane (Dach) and crystal structure of $[Cu(Dach)_2(H_2O)]Cl_2$, J. Mol. Struct. 1137 (2017) 784–791.
[28] R. Patela, N. Singha, K. Shuklaa, J. Niclós-Gutiérrezb, S. Astineirasb, V. Vaidyanathanc, B. Unni Nairc, Characterization and biological activities of two copper(II) complexes with diethylenetriamine and 2,2′-bipyridine or 1, 10-phenanthroline as ligands, Spectrochim. Acta Part A 62 (2005) 261–268.
[29] B. Agrahari, S. Layek, S. Kumari, R. Ganguly, D.D. Pathak, Synthesis, characterization and crystal structure of Cu(II) complex of *trans*-cyclohexane-1,2-diamine: application in synthesis of symmetrical biaryls, J. Mol. Struct. 1134 (2017) 85–90.
[30] F. Abu Saleemh, S. Musameh, A. Sawafta, P. Brandao, C.J. Tavares, S. Ferdov, A. Barakat, A. Al Ali, M. Al-Noaimi, I. Warad, Diethelenetriamine/diamines/copper (II) complexes [Cu(dien)(NN)]Br 2: synthesis, solvatochromism, thermal, electrochemistry, single crystal, Hirshfeld surface analysis and their antibacterial activity, Arab. J. Chem. 10 (2016) 845.
[31] M.Gh. Amiri, H. Golchoubian, Solvatochromism, thermochromism and density functional theory studies of Copper(II) complexes containing hemilabile tetradentate ligand, J. Mol. Struct. 1165 (2018) 196–205.
[32] S.I. Noro, N. Yanai, S. Kitagawa, T. Akutagawa, T. Nakamura, Binding Properties of Solvatochromic Indicators [Cu(X)(acac)(tmen)](X = PF6− and BF4−, acac− = Acetylacetonate, tmen = N, N, N′,N′-Tetramethylethylenediamine) in Solution and the Solid State, Inorg. Chem. 47 (2008) 7360–7365.
[33] Hamid Golchoubian, Razieh Samimi Solvato- and thermochromism study in oxalato-bridged dinuclear copper(II) complexes of bidentate diamine ligands, Polyhedron 128 (2017) 68–75.
[34] L. Rostami, H. Golchoubian, Synthesis, crystal structure and chromotropism study of copper complexes containing tridentate and pseudo halide ligands; amide linkage isomerism, Inorg. Chim. Acta 462 (2017) 215–222.
[35] I. Warad, S. Musameh, I. Badran, N.N. Nassar, P. Brandao, C.J. Tavares, A. Barakat, Synthesis, solvatochromism and crystal structure of trans-$[Cu(Et_2NCH_2CH_2NH_2)_2H_2O](NO_3)_2$ complex: experimental with DFT combination, J. Mol. Struct. 1148 (2017) 328–338.
[36] P. Inamdar, R. Chauhan, J. Abraham, A. Sheela, DNA interaction and cytotoxic activity of copper complex based on tridentate hydrazone derived ligand and nitrogen donor heterocycle, Inorg. Chem. Comm. 67 (2016) 67–71.
[37] Z. Shokohi-pour, H. Chiniforoshan, A. Abbas, M. Borojeni, B. Notash, A novel Schiff base derived from the gabapentin drug and copper (II) complex: Synthesis, characterization, interaction with DNA/protein and cytotoxic activity, J. Photochem. Photobiol. B Biol. 162 (2016) 34–44.
[38] M.P. Kesavan, G.G. Vinoth Kumar, J. Dhaveethu Raja, K. Anitha, S. Karthikeyan, J. Rajesh, DNA interaction, antimicrobial, antioxidant and anticancer studies on Cu (II) complexes of Luotonin A, J. Photochem. Photobiol. B Biol. 167 (2017) 20–28.
[39] I. Warad, F.F. Awwadi, M. Daqqa, A. Al Ali, T.S. Ababneh, T.M.A. AlShboul, T.M.A. Jazzazi, F. Al-Rimawi, T.B. Hadda, Y.N. Mabkhot, New isomeric $Cu(NO_2\text{-}phen)_2Br]Br$ complexes: Crystal structure, Hirschfeld surface, physicochemical, solvatochromism, thermal, computational and DNA-binding analysis, J. Photochem. Photobiol. B Biol. 171 (2017) 9–19.
[40] B. Gli ic, J. Runic, T. Tomic, H. Wadepohl, A. Veselinovic, I.M. Opsenica, M.I. Djuran, Synthesis, cytotoxic activity and DNA-binding properties of copper(II) complexes with terpyridine, Polyhedron 139 (2018) 313–322.
[41] D. Serre, S. Erbek, N. Berthet, X. Ronot, F. Thomas, Copper(II) complexes of N3O tripodal ligands appended with pyrene and polyamine groups: anti-proliferative and nuclease activities, J. Inorg. Biochem. 179 (2018) 121–134.
[42] F. Carlos, M. Nunes, B. Iglesias, P. Zambiazi, M. Hörner, G. de Moraes, G. Machado, R. Ribeiro, F. Nunes, Fluorenyl-Schiff-base ligands and their dicopper(II) complexes Synthesis, structural and spectroscopic characterization and DNA binding assays, Polyhedron 144 (2018) 18–29.